Detailed Numerical Study on the Aerodynamic Behavior of a Gurney Flapped Airfoil in the Ultra-low Reynolds Regime

Mahzad Khoshlessan[1], Seyed Mohammad Hossein Karimian[1]

ABSTRACT: The addition of Gurney flap changes the nature of flow around airfoil by producing asymmetric Von-Karman vortex in its wake. Most of the investigations on Gurney flapped airfoils have modeled the flow using a quasi-steady approach, resulting in time-averaged values with no information on the unsteady features of the flow. Among these, some investigations have shown that quasi-steady approach does a good job on predicting the aerodynamic coefficients and physics of flow. Previous studies on Gurney flap have shown that the calculated aerodynamic coefficients such as lift and drag coefficients from quasi-steady approach are in good agreement with the time averaged values of these quantities in time accurate computations. However, these investigations were conducted in regimes of medium to high Reynolds numbers where the flow is turbulent. Whether this is true for the regime of ultra-low Reynolds number is open to question. Therefore, it is deemed necessary to examine the previous investigations in the regime of ultra-low Reynolds numbers. The unsteady incompressible laminar flow over a Gurney flapped airfoil is investigated using three approaches; namely unsteady accurate, unsteady inaccurate, and quasi-steady. Overall, all the simulations showed that at ultra-low Reynolds numbers quasi-steady solution does not necessarily have the same correlation with the time averaged results over the unsteady accurate solution. In addition, it was observed that results of unsteady inaccurate approach with very small time steps can be used to predict time-averaged quantities fairly accurate with less computational cost.

KEYWORDS: Gurney flap, Ultra-low Reynolds number, NACA 0008 airfoil, Transient behavior, Incompressible flow, Laminar flow.

INTRODUCTION

Gurney flap (GF) is a tab of small height deployed at the trailing edge of the airfoil normal to the chord line at the pressure side. In the present paper, the effect of different numerical approaches on the aerodynamic behavior of a NACA 0008 airfoil equipped with a GF in laminar incompressible flow is investigated. GF is a simple device previously used on race cars, which is found to be useful in terms of providing the required downforce. Liebeck (1978) conducted an experimental study of the GF on a Newman airfoil in Douglas Long Beach low-speed wind-tunnel at Reynolds number based on cylinder diameter (Re_D) of 3×10^6. The results showed that the GF would provide higher value of maximum lift coefficient (C_L), increased lift at a specific angle of attack, and reduced drag at a specific C_L. The author hypothesized that the flow is composed of 2 counter-rotating vortices at the back side of the GF and a recirculating region upstream the flap. Later, this flow feature was also observed at low Reynolds number in a water tunnel by Neuhart and Pendergraft (1988).

Li *et al.* (2002), Myose *et al.* (1996), and Giguere *et al.* (1997) studied the effects of GF on the aerodynamic performance of various airfoils. Their results showed that the effect of GF is to substantially increase the maximum C_L and to reduce the stall angle. In addition, the zero-lift angle of attack becomes more negative with the increase in GF height. Overall, their results suggest that the effect of the GF is to increase the effective camber of the airfoil. Jeffrey *et al.* (2000) conducted an experimental study

over a single-element wing using laser Doppler anemometry along with pressure and force measurements. Based on the study performed by these authors, the time-averaged flow downstream a GF consists of 2 counter-rotating vortices, but the instantaneous flow structure actually consists of a wake of alternately shed vortices. Troolin *et al.* (2006) investigated the wake structure using time-resolved particle image velocimetry. They showed that 2 distinct vortex-shedding modes exist in the wake. The dominant mode resembles a Karman vortex street behind an asymmetric bluff body. The second mode is caused by the intermittent shedding of recirculating region upstream the flap, which becomes more coherent with the increase in the angle of attack. Manish *et al.* employed a compressible Reynolds-averaged Navier-Stokes (RANS) solver using Baldwin-Lomax turbulence model for the prediction of flow over NACA 0011 and NACA 4412 airfoils with different GF heights. All the computations in their study for NACA 4412 airfoil were performed for free-stream Mach number of 0.20 and chord Reynolds number of 2.0 million; those for NACA 0011 airfoil were carried out for Mach number of 0.14 and chord Reynolds number of 2.2 million.

They carried out their computations with the assumption that the flow is steady. The computed force coefficients had a good correlation with the experiment. But it was observed that the difference between numerical and experimental results increases with angle of attack and flap height. Ashby (1996) conducted experimental and computational studies to investigate the effects of lift-enhancing tabs on a multi-element airfoil. All of the computations were obtained using 2-D, incompressible RANS solver in the steady-state mode implementing the Spalart-Allmaras turbulence model. Good agreement was achieved between computed and experimental results, particularly for cases where no flow separation exists on the flap upper surface. However, poor agreement was obtained for configurations where significant flow separation exists over the flap upper surface. Overall, the computed results predicted all of the trends observed in the experimental data quite well.

Date and Turnock (2002) carried out a detailed computational study on the quasi-steady and periodic performance of NACA 0012 airfoil equipped with GFs with a flap height-to-chord ratio of 2 and 4% using the incompressible RANS solver and implementing the standard k-ε turbulence model at Reynolds number of 0.85×10^6. They showed that the time-averaged performance is identical to the performance predicted by the quasi-steady solution, showing the same correlation with

the experimental data. According to their investigation, when periodic performance of airfoil is of secondary importance, the quasi-steady solution can be used to obtain estimates of airfoils, mean performance for practical purposes. According to the study performed by Date and Turnock (2002), quasi-steady approach has the same prediction of mean performance as time accurate computations.

Based on the experimental studies in the literature regarding Gurney-flapped airfoils, the addition of flap originates vortex shedding, and the flow becomes unsteady (Jeffrey *et al.* 2000; Troolin *et al.* 2006). As a result, all computations should be performed in unsteady mode. Nevertheless, many numerical computations assume a steady flow and use steady-state computations for the prediction of the flow (Singh *et al.* 2007; Ashby 1996; Jang *et al.* 1992; Ross *et al.* 1995). To the best of our knowledge, all of the studies in the literature are performed at medium-to-high Reynolds number flow regimes. However, less attention has been paid to the performance of GF at ultra-low Reynolds number (Re below 10,000) flow regime where the boundary layer, wake characteristics, and other flow features are different.

The regime of ultra-low Reynolds number has recently received special interest and has been the subject of many computational and experimental researches. According to the studies conducted in this flow regime, it has many applications in the analysis of aerodynamics at small physical scales (insect-sized aircraft), especially flight of Micro-Air Vehicles (MAVs). The choice of airfoil plays an important role in the design of aircraft suitable for low-speed aerodynamics. Also the payload, range, and endurance of the low-speed aircraft are limited by the performance of their high-lift systems (Storms and Jang 1994). Some investigations conducted a parameter study for analysis and design of airfoils suitable for ultra-low Reynolds numbers. Kunz (2003), in their computational study of ultra-low Reynolds numbers (between 1,000 and 6,000), developed an automated optimal design tool for 2-D airfoils at ultra-low Reynolds numbers and a hybrid method for the automated design and analysis of micro-rotors. Abdo (2004), in their study, presented an efficient numerical method for the incompressible flows past airfoils at low Reynolds numbers. Their analysis was based on a pseudo-time integration method using artificial compressibility to accurately solve the Navier-Stokes equations. They obtained solutions for airfoils at various incidences and very-low Reynolds numbers between 400 and 6,000. Furthermore, the generation of high lift can

lead to steeper take-off ascent, increase in the climb lift-to-drag ratio, and fuel economy (Tejnil 1996). Therefore, the choice of an efficient high lift device would also be of great importance. GF is a good candidate to maintain high-lift coefficient required for approach and landing (Storms and Jang 1994) and is a mechanically-simple and cost-effective device in contrast with other complex multi-element high-lift ones, being used to control the flow in combination with other elements (Schatz *et al.* 2004). Thus, the motivation for this study was: (a) to model a Gurney-flapped airfoil at ultra-low Reynolds flow regime, since the understanding of aerodynamic behavior of the airfoil at this Reynolds number would be helpful for the design of low-speed aircraft; and (b) to investigate whether steady-state solution can still be used to predict mean performance of unsteady flow around Gurney-flapped airfoils at ultra-low Reynolds regime.

To this end, the Mass Corrected Interpolation Method (MCIM) algorithm of Alisadeghi and Karimian (2010) is employed for the solution of flow over a NACA 0008 Gurney-flapped airfoil. This method is one of the most robust ones for incompressible flow calculation that provides an efficient and accurate tool for solving practical engineering problems (Alisadeghi and Karimian 2010) and has been previously validated for internal flows (Alisadeghi and Karimian 2010), including Taylor problem, inviscid converging-diverging nozzle, and the lid-driven cavity, as well as for external flows (Khoshlessan *et al.* 2013; Khoshlessan 2013), including steady and unsteady flows over a circular cylinder section and unsteady flow over a NACA 0012 airfoil.

Three implicit time-marching approaches are implemented for the prediction of flow over a Gurney-flapped airfoil: (a) unsteady accurate, which refers to the solution in which linearization iterations are performed at each time step (Δt); (b) unsteady inaccurate, which refers to the solution in which no linearization iteration is performed at each Δt; and (c) quasi-steady, which refers to the solution in which the transient term is eliminated from the Incompressible Navier-Stokes (INS) equations, *i.e.* very-large time steps are used. Grid refinement and time-step independence studies are conducted to ensure the generation of accurate solution. Results obtained from these approaches are studied in detail and compared with each other. Moreover, the effect of linearization convergence criterion (e) on the time accurate solution and the sensitivity of all calculated parameters to the other values of e are investigated. As it will be seen, the present paper concludes that, in contrast to high Reynolds numbers flow, the quasi-steady solution cannot

be used to correctly predict the mean aerodynamic behavior of a Gurney-flapped airfoil at ultra-low Reynolds numbers. It will be also shown that the unsteady inaccurate approach with very-small time steps can be used to fairly predict the time-averaged quantities accurately with 1/3 of computational cost needed for unsteady accurate calculations.

In addition, the governing equations are implicitly formulated and solved using direct methods. Two different direct solvers are examined here to study their effect on the required memory and speed up of the solution.

NUMERICAL ALGORITHM AND GOVERNING EQUATIONS

In this study, the MCIM (Alisadeghi and Karimian 2010) is employed for solving 2-D incompressible flows on structured grid systems. The present algorithm can be classified among the collocated grid schemes in control-volume-based methods in which 2 different velocity components at cell faces are defined to suppress the possible checkerboard problem in the solution domain. In the present approach, conservation equations are formed for each control volume throughout the solution domain. In addition, a fully-coupled formulation is used. The linear system of equations obtained in these algorithms is solved using a direct sparse solver. The transient term is modeled using a first-order backward difference in time. Convective term is linearized by lagging the stream-wise velocity and modeled so that it would cause the upstream value of velocity u_{up} to affect u_{ip} strongly, when convection is dominant. Also, the convective term is modeled using a first-order backward differencing in the upstream direction.

The computational domain is discretized into a number of quadrilateral elements, and all primitive variables are located at the vertices of these elements. A local non-orthogonal coordinate system (s,t) is defined inside each element. Medians within the element divide it into 4 sub-control volumes (SCVs), as shown in Fig 1a. Each SCV is associated with an elemental node at its vertex, and each node is surrounded by 4 SCVs that form a control volume for the given node. Sub-control surfaces (SCSs) are the representative of boundary surfaces of the SCVs fallen inside the element, and the integration points (i_p) are the representative of the midpoint of the SCSs. Diffusion fluxes and pressure terms at the integration points are related to the nodal variables using bi-linear interpolation. Mass and the

convection fluxes at the i_p should be also related to the nodal values of velocity and pressure.
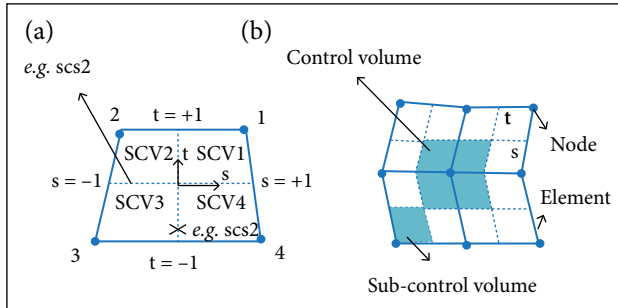
Figure 1. Definition of (a) element and (b) control volume and sub-control volume.

All primitive variables are located at the vertices of the elements and should be evaluated at the i_p to determine the flux at each SCS. Using the linear interpolation, any variable and its gradients within the element can be calculated. More details of the method by which these fluxes are defined at the i_p and the formation of the system of linearized equations and time-marching scheme can be found in Karimian and Schneider (1995, 1994) and Karimian (1994). Governing equations are the INS equations, and its integral form for SCV2 in Fig. 1, for instance, is given by:

$$\int_{SCV2} \frac{\partial Q}{\partial t} dV + \int_{SCS1\&2} (Eds_x + Fds_y) =$$
$$= \int_{SCS1\&2} (Gds_x + Hds_y),$$

where: dV represents volume differential; ds_x and ds_y represent components of the outward vector normal to the surface; SCS denotes the inner sub-control surface associated with SCV2; Q, E, F, G, and H are defined as follows:

$$Q = \begin{pmatrix} 0 \\ \rho u \\ \rho v \end{pmatrix}, \quad E = \begin{pmatrix} (\rho u) \\ (\rho u)u + p \\ (\rho u)v \end{pmatrix}, \quad F = \begin{pmatrix} (\rho v) \\ (\rho v)u \\ (\rho v)v + p \end{pmatrix},$$

$$G = \begin{pmatrix} 0 \\ \tau_{xx} \\ \tau_{xy} \end{pmatrix}, \quad H = \begin{pmatrix} 0 \\ \tau_{xy} \\ \tau_{yy} \end{pmatrix}$$

$$\tau_{xx} = 2\mu \frac{\partial u}{\partial x}, \quad \tau_{yy} = 2\mu \frac{\partial v}{\partial y}, \quad \tau_{xy} = \tau_{yx} = \mu \left(\frac{\partial u}{\partial y} + \frac{\partial v}{\partial x} \right)$$

where: ρ is the density; u is the convected stream-wise velocity; v is the convected transverse velocity; μ is the dynamic viscosity.

The volume integral of the transient term is modeled using a first-order backward difference in time. Any integral argument, i.e. E, F, G, and H, is approximated by its average value over the SCS, which is evaluated at its midpoint location (i_p). For diffusion flux vectors G and H, bi-linear interpolation is used to directly evaluate the components of stress tensor (Karimian and Schneider 1995, 1994; Karimian 1994). For convective flux vectors E and F, pressure is evaluated using bi-linear interpolation, and the momentum fluxes are linearized with respect to mass fluxes (ρu) and (ρv). Velocity components u and v in mass fluxes are called integration point mass-conserving velocities, being denoted by a hat, i.e. $\rho \hat{u}$ and $\rho \hat{v}$. Other values of u and v in the momentum fluxes, which are convected by the mass fluxes through the control-volume surface, are called integration point convected velocities. Mass-conserving and convected velocities are cell-face velocities. Details of the modeling of the cell-face velocities are represented in Alisadeghi and Karimian (2010) in detail. It should be noted that, since Navier-Stokes equations are non-linear by nature, and in order to have a linear system of equations, convection terms in momentum equations are linearized by lagging the stream-wise velocity. This means that the mass fluxes (ρu and ρv) in convection term are calculated from previous iteration, which introduces an error to the solution. Therefore, it is necessary to perform the linearization iteration at each Δt in order to reduce the linearization error to the lowest possible amount. The ε used to stop the linearization iteration process is given by Eqs. 3 and 4, in which z_j is the jth unknown variable. For all of the solutions over a circular cylinder shown here, ε is set equal to 0.1%.

$$\left(\frac{\sum_{j=1}^{3} \sum_{i=1}^{N} \left| \frac{(z_j)_i - (z_j)_i^o}{Z_j} \right|^2}{3 \times N} \right)^{0.5} < \varepsilon$$

where:

$$Z_j = \left(\frac{\sum_{i=1}^{N} |(z_j)_i|^2}{N} \right)^{0.5}$$

Three approaches are implemented for all the simulations performed in the present study. Comparison between these approaches are made for the case of Gurney-flapped airfoil. These approaches are as follows:

- Unsteady accurate solution (UAS), in which linearization iterations are performed at each Δt. The ε used to stop linearization iteration process is defined by Eqs. 3 and 4.
- Unsteady inaccurate solution (UIS), in which no linearization iteration is performed at each Δt.
- Quasi-steady solution (QSS), in which the transient term is eliminated from the INS equations and is considered equivalent to UIS, with $\Delta t \rightarrow \infty$.

BOUNDARY CONDITIONS

Velocity inlet boundary condition is specified at the inflow boundary, *i.e.* $u = U_\infty cos\alpha$ and $v = U_\infty sin\alpha$, where U_∞ is the free stream velocity. Pressure outlet boundary condition is specified at the outflow boundary, *i.e.* $\partial v / \partial s = 0$ and $p_{outflow} = P_\infty$. No-slip boundary condition is employed at all walls, *i.e.* velocities are set equal to 0 on all boundary nodes. GF is considered as a single flat plate without thickness; on its both sides, no-slip boundary condition is applied.

IMPLEMENTATION OF BAND SOLVER AND DIRECT SPARSE SOLVER

As mentioned before, in the present numerical study, the governing equations are implicitly formulated, which leads to the formation of a system of linearized equations that should be solved at each Δt (UAS approach). Since the number of unknown variables is typically very large, solving the resulted coefficient matrix has a significant impact on computational time. To reduce the amount of required memory and to speed up the convergence rate in the iterative process for the solution of the system of equations, the following tasks and their effects are examined:

- Implementation of band solver.
- Implementation of a direct sparse solver.

The details about the band solver are not given here and can be found in Khoshlessan *et al.* (2013) and Khoshlessan (2013). Only Sparse solver is discussed, as it is used in all simulations. It should also be noted that all the simulations are executed in serial mode in the present study.

DIRECT SPARSE SOLVER

Note that the main part of the present study is dedicated to unsteady flows. Therefore, very-fine grids are required to predict time evolution of the wake and the flow periodicity. As a result, the number of unknown variables will be very large, which results in a very large coefficient matrix. This leads to a noticeable increase in both CPU time and required memory, especially when extremely intensive computations are necessary to be carried out with small time steps. To handle such cases, a direct sparse solver called BLOCKPACK (Karimian 1994) is implemented instead of the band solver to solve the renumbered band matrix. In order to test the efficiency of the sparse solver, the case of unsteady flow over a circular cylinder at $Re_D = 100$ is examined. Table 1 shows the comparison of CPU time taken to complete 7,500 time steps to reach the solution at $t = 7.5$ s using band solver and direct sparse solver.

As illustrated in Table 1, the average time needed for each linearization iteration is reduced to 20 s for sparse solver as compared to 9 min for band solver. Thus, the amount of CPU time taken to complete 7,500 time steps using sparse solver is 1/27 of that of the band solver (41.67/1,125). As can be seen, the implementation of direct sparse solver has led to significant speed up in convergence rate and saving in computational time.

ALGORITHM VALIDATION

For the validation of the present algorithm, 2 test cases are studied. In both, cases results are compared against other numerical and experimental results available in the literature (Berthelsen and Faltinsen 2008; Russel and Wang 2003; Linnick and Fasel 2005; Herfjord 1996; Calhoun 2002; Medjroubi 2011; Coutanceau and Bouard 1977; Tritton 1959). All the simulations in validation section are performed using the UAS approach. The first test case is steady flow over a circular cylinder at $Re_D = 40$. Grid refinement study is conducted to ensure that there is enough near wall resolution, and the obtained results are accurate. The numerical grid used for the simulation is an

Table 1. Comparison of CPU time taken to reach periodic state of unsteady flow over a circular cylinder at $Re_D = 100$ with $\Delta t = 10^{-3}$ s using band solver and direct sparse solver.

Solver	Average time needed for each linearization iteration	Average number of linearization iterations in each Δt	CPU Time (h) needed to complete 7,500 time steps to reach the solution at $t = 7.5$ s
Band	9 min	1	1,125
Sparse	20 s	1	41.67

O-type grid topology, composed of quadrilateral elements. The cylinder is located at $(x, y) = (D/2, 0)$, where D is the cylinder diameter. The far-field boundary is located at 20 chords (C) away from the center of the cylinder in all computations. In this case, grid refinement study is performed based on 2 independent radial (N_r) and angular (N_θ) directions, and the sensitivity of the calculated drag force with change in grid resolution is studied. Three different mesh counts with sizes of 220×40, 220×60, and 220×80, in N_r, and with sizes of 180×60, 220×60, and 260×60, in N_θ, are used for this purpose. Drag coefficient (C_D) calculated from the steady-state solution and the corresponding relative error (E) on these grids are reported in Tables 2 and 3, which are defined as:

$$\Delta_{j,j-1} = \left| C_{D_j} - C_{D_{j-1}} \right| \tag{5}$$

$$E_{i,j-1} = \Delta_{i,j-1} / C_{D_j} \tag{6}$$

Table 2. Angular grid independence study at Re_D= 40 (N_θ = 220).

Grid	N_r	C_D	$E_{i,i-1}$ (%)
1	40	1.5513	--
2	60	1.5505	0.0516
3	80	1.5502	0.0194

Table 3. Angular grid independence study at Re_D= 40. (N_r = 60)

Grid	N_θ	C_D	$E_{i,i-1}$ (%)
1	180	1.5505	--
2	220	1.5483	0.1421
3	260	1.5478	0.0323

In Tables 2 and 3, indices 1, 2, and 3 refer to large, medium, and fine grids used for grid independence study. In Table 2, E_{21} and E_{32} of C_D are 0.05 and 0.02, respectively, which are very low. The grid refinement study provides details of fine mesh (220×80) compared to medium (220×60) and coarse (220×40) meshes. Mesh refinement study performed on the coarse, medium, and fine grids on CD shows very little variation when increasing mesh size, leaning towards their limiting trends. Therefore, 60 nodes in radial direction would be the best choice here. The first grid node should be located at $0.00044D$ away from the cylinder surface for the mesh to be able to capture details of the flow field with this number of grid points. With the same argument, one can conclude that, based on grid refinement study for fine (260×60), medium (220×60), and coarse (180×60) meshes shown in Table 3, the

medium grid (220×60) is enough tin in the angular direction. Therefore, the best grid to obtain grid independent results in this case is the medium one.

In the next step, the present results are compared with others reported in the literature (Berthelsen and Faltinsen 2008; Russel and Wang 2003; Linnick and Fasel 2005; Herfjord 1996; Calhoun 2002; Medjroubi 2011; Coutanceau and Bouard 1977; Tritton 1959). Drag force and geometrical parameters of the steady flow structure around a circular cylinder, defined in Fig. 2 and calculated on the 220×60 grid, are shown in Table 4, where they are compared with other experimental and numerical
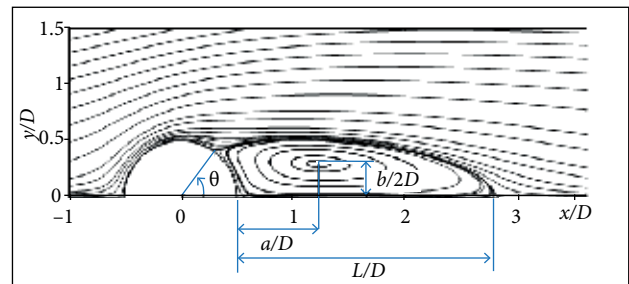
Figure 2. Nomenclature of the geometrical parameters for the flow over a circular cylinder at Re_D = 40 (Berthelsen and Faltinsen 2008).

Table 4. Comparison of geometrical parameters for the flow over a motionless cylinder at Re_D = 40.

Reference	L/D	a/D	b/D	Θ(°)	C_D
Berthelsen and Faltinsen (2008)	2.29	0.72	0.6	53.9	1.59
Russel and Wang (2003)	2.29	--	--	53.1	1.6
Linnick and Fasel (2005)	2.28	0.72	0.6	53.6	1.54
Herfjord (1996)	2.25	0.71	0.6	51.2	1.6
Calhoun (2002)	2.18	--	--	54.2	1.62
Medjroubi (2011)	2.21	0.7	0.59	53.8	1.6
Coutanceau and Bouard* (1977)	2.13	0.76	0.59	53.5	--
Tritton* (1959)	--	--	--	--	1.57
Average of other numerical results	2.25	0.7125	0.5975	53.3	1.592
Error of the average of other numerical results with respect to experiment (%)	5.6	6.6	1.3	0.4	1.4
Present study	2.25	0.72	0.6	53.8	1.55
Present study with respect to experiment (%)	5.6	5.3	1.7	0.56	1.3

*Experimental results.

results (Berthelsen and Faltinsen 2008; Russel and Wang 2003; Linnick and Fasel 2005; Herfjord 1996; Calhoun 2002; Medjroubi 2011; Coutanceau and Bouard 1977; Tritton 1959). In order to compare the efficiency of the present method concerning other numerical methods, the average of error in other numerical results is calculated. Thus, the error of the average of other numerical results as well as the error of the present data, with respect to the experiment (%), are compared. As can be seen, the relative error of the present results for L/D, a/D, b/D, θ/D, and C_D are 5.6; 5.3; 1.7; 0.56 and 1.3, respectively, with respect to the experiment, where L is the length of the recirculation region; a is the length of the center of recirculation region; b is the width of the center of recirculation region; θ is the separation angle. These errors are less than or about the same amount as compared to the relative error in the average of other numerical results, i.e. 5.6; 6.6; 1.3; 0.4 and 1.4 with respect to experiment. Thus, it can be concluded that the present algorithm predicts the details of the steady external flows over 2-D bodies very well as compared to other numerical results.

A second test case is performed to validate the present algorithm for the solution of unsteady flow that, over a circular cylinder at $Re_D = 100$, at which Von-Karman street is produced in its wake, is used for this purpose. The same grid of 220×60 points is adopted for the solution of the unsteady flow based on the grid study performed in previous section. This case is solved with different time steps to ensure Δt independent solution. During the transient regime, solution linearization iterations are performed at each Δt (refer to Eqs. 3 and 4 for definition). Solution is continued until the fully periodic state is achieved. Strouhal number (St), mean drag coefficient ($C_{D,m}$), amplitude drag coefficient ($C_{D,a}$), and amplitude lift coefficient ($C_{L,a}$) are extracted from the numerical results obtained from the present solution. Time steps of 10^{-3}; 10^{-4}, and 5×10^{-5} s are considered here, and the corresponding results are shown in Table 5. The change in time step from 10^{-3} to 10^{-4} s has altered St, $C_{D,m}$, $C_{D,a}$, and $C_{L,a}$ by 1.93; 0.44; 3.25 and 1.12%, respectively, while a decreasing time step from 10^{-4} to 5×10^{-5} s has changed St, $C_{D,m}$, $C_{D,a}$, and $C_{L,a}$ by only 0.175; 0.004; 0.165 and 0.35%,

respectively. Relative error in the change of parameters listed in Table 5 from time step of 10^{-4} to 5×10^{-5} s are less than 1%. If a relative error of less than 1% is fine enough, then the time step of $\Delta t = 10^{-4}$ s is an appropriate value to accurately capture unsteady flow field around a circular cylinder at $Re_D = 100$.

The results are compared with those of the other numerical or experimental studies (Russel and Wang 2003; Calhoun 2002; Ding et al. 2007; Liu et al. 1998; Xu and Wang 2006; Williamson 1989) available in the literature in Table 6. In order to compare the efficiency of the present method as compared to other numerical methods, the average of error in other numerical results is calculated. The maximum relative error of the other numerical results with respect to their average (%) and the error of present data with respect the average of other numerical results

Table 6. Unsteady flow past circular cylinder at $Re_D = 100$.

Reference	St	$C_{D,m}$	$C_{D,a}$	$C_{L,a}$
Ding et al. (2007)	0.166	1.356	0.01	0.287
Russel and Wang (2003)	0.169	1.38	0.007	0.3
Liu et al. (1998)	0.165	1.35	0.012	0.339
Calhoun (2002)	0.175	1.33	0.014	0.298
Xu and Wang (2006)	0.171	1.42	0.013	0.34
Williamson** (1989)	0.164	--	--	--
Average of other numerical results	0.1692	1.3672	0.0112	0.3128
Max. relative error in the above results with respect to average listed above (%)	3.42	3.8	37.5	8.69
Error of the average of numerical results with respect to experiment (%)	3.2	--	--	--
Present study ($\Delta t=10-4s$)	0.1711	1.37776	0.0123	0.2868
Error* (%)	1.12	0.77	9.8	8.3
Present study with respect to experiment (%)	4.3	--	--	--

*This is error of the results of the present study ($\Delta t = 10^{-4}$ s) with respect to the average of results listed above; **Experimental study.

Table 5. Time step independence study for unsteady flow past circular cylinder at $Re_D = 100$.

Case	Present study	St	$E_{i,i-1}$(%)	$C_{D,m}$	$E_{i,i-1}$ (%)	$C_{D,a}$	$E_{i,i-1}$(%)	$C_{L,a}$	$E_{i,i-1}$ (%)
1	($\Delta t = 10^{-3}$ s)	0.1678	--	1.372	--	0.0127	--	0.2900	--
2	($\Delta t = 10^{-4}$ s)	0.171	1.93	1.378	0.44	0.0123	3.25	0.2868	1.12
3	($\Delta t = 5 \times 10^{-5}$ s)	0.171	0.175	1.378	0.0	0.0121	0.165	0.2858	0.35

are compared. As can be seen in Table 6, the relative errors of the present results for St, $C_{D,m}$, $C_{D,a}$, and $C_{L,a}$ with respect to the average of other numerical results (Russel and Wang 2003; Calhoun 2002; Ding *et al.* 2007; Liu *et al.* 1998; Xu and Wang 2006; Williamson 1989) (1.12; 0.77; 9.8 and 8.3) are less than the maximum relative error in other numerical results (Russel and Wang 2003; Calhoun 2002; Ding *et al.* 2007; Liu *et al.* 1998; Xu and Wang 2006; Williamson 1989) and their average values (3.42; 3.48; 37.5 and 8.69).

Again, from the results obtained here, one can conclude that the present algorithm predicts excellently the details of external unsteady flows over 2-D bodies as well. The relative error of St for the present results and the average of other numerical results (Russel and Wang 2003; Calhoun 2002; Ding *et al.* 2007; Liu *et al.* 1998; Xu and Wang 2006; Williamson 1989) are 4.3 and 3.2, respectively with respect to experimental data (Table 6). The comparison presented in Table 6 shows that the present algorithm does a good job in predicting the St and aerodynamic coefficients for unsteady flow over a circular cylinder.

RESULTS

In this section, the MCIM algorithm of Alisadeghi and Karimian (2010) validated before for external flows over 2-D bodies is used for the analysis of laminar flow over a NACA 0008 airfoil fitted with GF. All of the simulations presented herein are performed by solving the INS equations with the assumption that the flow is laminar over the entire domain. Steady solutions are obtained when aerodynamic forces converge to their final value. Unsteady solutions are obtained after several periodic cycles, where the force coefficient time series reach a periodic state. Grid and time refinement studies are performed to ensure independent solutions. Grid refinement study is first performed in order to find proper number of grid points in different directions of the computational grid. Discussions on grid refinement study are given in the following subsection.

Numerical grid used for the simulation is a structured C-type grid topology. Gurney flapped NACA 0008 airfoil is located at $(x,y) = (C/2,0)$, and the far-field boundary is located at $20C$ away from the center of the airfoil in all directions. Uniform flow over the airfoil is from left to the right in the x-direction, and the entire domain is initialized using the undisturbed uniform flow at the far-field inlet boundary condition.

GRID REFINEMENT STUDY

Grid refinement study is conducted on a Gurney flapped airfoil with a flap height of $H_f = 4\%C$, at Reynolds number based on chord length (Re_C) of 2,000 and angle of attack $\alpha = 4°$. Grid resolution is changed in different regions of computational domain independently, *i.e.* inside the flap region (N_f), in the radial direction (N_η), along the chord (N_ξ), and in the wake (N_ζ) to ensure enough grid points in each direction. This will be of great importance to capture physics of the flow accurately. Figure 3 shows the schematic diagram of the computational grid around a Gurney flapped airfoil.
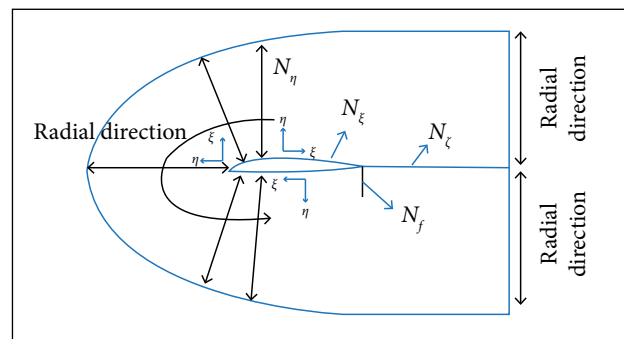
Figure 3. Schematic diagram of the computational grid.

It is important to note that the computational time of the unsteady accurate solution approach is much higher than that of the quasi-steady approach, due to the linearization iterations, which should be performed at each Δt in unsteady accurate solution approach. Therefore, quasi-steady approach is used in all simulations carried out in this section to avoid the extremely-intensive computational burden due to time accurate computations. Thus, the quasi-steady values of lift and drag coefficients are the parameters which their changes due to the grid refinement will be monitored in this study. In each test case, the number of grid points is changed in one direction, while the number of grid points in the other directions is kept constant. Grid refinement study is of great importance in order to reach an independent and accurate solution. Calculated force coefficients along with their relative errors computed on 12 grids with different resolutions are considered next. Note that, in the subsequent sections, the error of the lift coefficient (C_L) is calculated similarly to error of C_D, as defined in Eqs. 3 and 4.

Flap Grid Independence Study

As seen in Table 7, the relative error E_{21} of C_D and C_L is 0.3694 and 1.1894%, respectively, from the coarse grid to the medium

one, and E_{32} of C_D and C_L is 0.1353 and 0.0744%, respectively, from the medium grid to the finest one. From the coarsest grid to the finest one, the solution changes, and relative errors of both C_D and C_L are reduced, leaning toward their limiting trend. Therefore, N_f=30 would be the best choice here as the baseline resolution for all subsequent computations.

Table 7. Flap Grid Independence Study with $H_f/C = 4\%$ at $Re_C = 2,000$ and $\alpha = 4°$.

Grid	N_f	$N_\eta = 70$, $N_\xi = 100$, $N_\zeta = 80$			
		Lift data		Drag data	
		C_L	$E_{i,i-1}$	C_D	$E_{i,i-1}$
1	20	0.5445	--	0.08092	--
2	30	0.5381	1.1894	0.08122	0.3694
3	40	0.5377	0.0744	0.08133	0.1353

Radial Grid Independence Study

As seen in Table 8, relative errors of C_D and C_L are very small. The relative error E_{32} of C_D and C_L is approximately 0.012 and 0.074% from the medium grid to the finest one, and E_{21} of C_D and C_L is approximately 0.037 and 0.17% from the coarse grid to the medium one. Based on these data, one can conclude that C_D and C_L have reached their limiting values. Therefore, $N_\eta = 70$ would be the best choice here as the baseline resolution for all subsequent computations.

Table 8. Radial grid independence study with $H_f/C = 4\%$ at $Re_C = 2,000$, and $\alpha = 4°$.

Grid	N_η	$N_f = 30$, $N_\xi = 100$, $N_\zeta = 80$			
		Lift data		Drag data	
		C_L	$E_{i,i-1}$	C_D	$E_{i,i-1}$
1	60	0.539	--	0.08119	--
2	70	0.5381	0.1673	0.08122	0.0369
3	80	0.5377	0.0744	0.08123	0.0123

Chord Wise Grid Independence Study

As can be seen in Table 9, the relative error E_{32} of C_L is approximately 0.1485% from the medium grid to the finest one, and E_{21} of C_L is approximately 0.1858% from the coarse grid to the medium one, which shows that C_L has reached its limiting value. Regarding the relative error of C_D, we believe that, although E_{32} (0.0002) is larger than E_{21} (3×10^{-5}), both are small enough to accept that C_D has also reached to its limiting value, as can be seen in Table 9. Therefore, selection of the medium grid with $N_\xi = 100$ is an appropriate choice in this case.

Table 9. Chord wise grid independence study with $H_f/C = 4\%$ at $Re_C = 2,000$, and $\alpha = 4°$.

| Grid	N_ξ	$N_f = 30$, $N_\eta = 70$, $N_\zeta = 80$			
		Lift data		Drag data	
		C_L	$E_{i,i-1}$	C_D	$E_{i,i-1}$
1	80	0.5371	--	0.08119	--
2	100	0.5381	0.1858	0.08122	0.0369
3	120	0.5389	0.1485	0.08142	0.2456

Wake Grid Independence Study

As seen in Table 10, the relative errors of C_D and C_L are very small. The relative error E_{32} of C_D and C_L is approximately 0 and 0.0186% from the medium grid to the finest one, and E_{21} of C_D and C_L is approximately 0.0123 and 0.0186% from the coarse grid to the medium one. Based on these data, one can conclude that C_D and C_L have reached their limiting values. Therefore, the selection of the medium grid with $N_\zeta = 90$ is an appropriate choice in this case.

Finally, based on the error reduction achieved through grid refinements, a grid with $N_f = 30$, $N_\eta = 70$, $N_\xi = 100$, $N_\zeta = 90$ is selected for all the subsequent solutions of Gurney flapped airfoil. This grid is based on the medium cases which yield lift and drag coefficients with very small errors (within 0.2%) from the finest grids. Figure 4a shows the C-grid topology used for the computations, and Fig. 4b presents details of numerical grid used for the simulations in the flap region.

Table 10. Wake grid independence study with $H_f/C = 4\%$ at $Re_C = 2,000$, and $\alpha = 4°$.

Grid	N_ζ	$N_f = 30$, $N_\eta = 100$, $N_\xi = 80$			
		Lift data		Drag data	
		C_L	$E_{i,i-1}$	C_D	$E_{i,i-1}$
1	80	0.5381	--	0.08122	--
2	90	0.5382	0.0186	0.08121	0.0123
3	100	0.5383	0.0186	0.08121	0
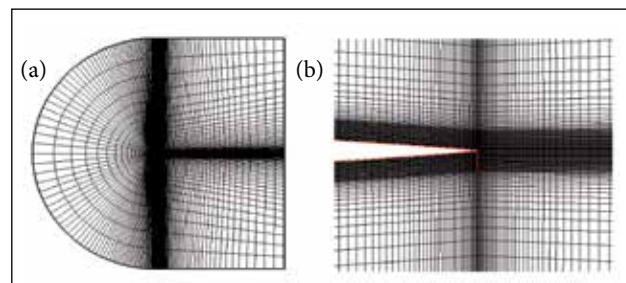
Figure 4. Details of computational grid (a) around the section and (b) inside the flap region.

SIMULATIONS OF FIXED GURNEY FLAPPED AIRFOIL

In the present section, the performance of the quasi-steady approach in comparison with unsteady accurate approach will be evaluated in the regime of ultra-low Reynolds numbers. Different approaches for the prediction of flow over a Gurney flapped airfoil will be investigated and compared with each other.

Simulations are carried out for a NACA 0008 airfoil with a flap to chord ratio of $H_f/C = 4\%$ at angles of attack of 3°, 4°, and 7° and at Reynolds number of 2,000 using the 3 approaches introduced in the section "Implementation of band solver and direct sparse solver".

Parameters under consideration in the present study are St, mean lift coefficient ($C_{L,m}$), $C_{D,m}$, $C_{L,a}$, and $C_{D,a}$, reported in Tables 11 to 13. All the calculated parameters are obtained from C_L and C_D time series, once the computed flow field has converged to a periodic solution. The linearization convergence criterion used to stop linearization iteration process for all the calculations summarized in Tables 11 to 13 is $\varepsilon = 0.1\%$. To ensure a Δt independent solution for UAS approaches at each angle of attack, variation of St, $C_{L,m}$, $C_{D,m}$, $C_{L,a}$, and $C_{D,a}$ is monitored for a variety of time steps to achieve accurate

transient solutions for the prediction of unsteady flow structure and aerodynamics of a Gurney flapped airfoil.

TIME STEP INDEPENDENCE STUDY

Tables 11 to 13 illustrate the sensitivity of the calculated quantities using UAS approach to different time steps ranging from $\Delta t = 10^{-3}$ s to $\Delta t = 10^{-5}$ s. As seen in these tables, $C_{L,m}$, $C_{D,m}$, and St extracted from the numerical results calculated using UAS approach show a monotone and asymptotic convergence leaning toward their limiting trend as Δt decreases from $\Delta t = 10^{-3}$ s to $\Delta t = 10^{-5}$ s. The relative errors in $C_{L,m}$, $C_{D,m}$, and St from $\Delta t = 10^{-3}$ s to $\Delta t = 10^{-5}$ s are reduced from 2.59 to 1.37%, 0.33 to 0.15%, and 78.9 to 1.53% at $\alpha = 3°$; 8.5 to 1.16%, 1.33 to 0.14%, and 16.7 to 1.17% at $\alpha = 4°$; and 19.03 to 0.74%, 7.75 to 0.23%, and 10.7 to 0.17% at $\alpha = 7°$, respectively. The E_{43} of $C_{L,m}$, $C_{D,m}$, and St is 1.37; 0.15 and 1.57% at $\alpha = 3°$; 1.16; 0.14 and 1.17% at $\alpha = 4°$; and 0.74; 0.23 and 0.17% at $\alpha = 7°$, respectively, which are fine enough and in the same order of magnitude.

Moreover, amplitude lift and drag coefficients extracted from the numerical results of UAS approach also show a monotone and asymptotic convergence as time step decreases from

Table 11. Unsteady accurate solution at Re_C = 2,000, α = 3° with H_f/C = 4%, ε = 0.1%.

Case	Δt (s)	$C_{L,m}$	$E_{j,i-1}$	$C_{L,a} \times 10^{-2}$	$E_{j,i-1}$	St	$E_{j,i-1}$	$C_{D,m}$	$E_{j,i-1}$	$C_{D,a} \times 10^{-3}$	$E_{j,i-1}$
4	0.00001	0.50659	1.37	0.3215	29.9	1.570	1.53	0.07858	0.15	0.5056	29.6
3	0.00005	0.49963	1.59	0.2253	41.2	1.546	2	0.07846	0.19	0.3561	41.7
2	0.0001	0.49170	2.59	0.1325	99.5	1.515	78.9	0.07832	0.33	0.2075	99.5
1	0.001	0.47897	--	0.00069	--	0.319	--	0.07806	--	0.001068	--

Table 12. Unsteady accurate solution at Re_C = 2,000, α = 4° with H_f/C = 4%, ε = 0.1%.

Case	Δt (s)	$C_{L,m}$	$E_{j,i-1}$	$C_{L,a} \times 10^{-2}$	$E_{j,i-1}$	St	$E_{j,i-1}$	$C_{D,m}$	$E_{j,i-1}$	$C_{D,a} \times 10^{-3}$	$E_{j,i-1}$
4	0.00001	0.60256	1.16	0.6978	15.3	1.5448	1.17	0.08256	0.14	1.2289	15.2
3	0.00005	0.59558	1.20	0.5909	16.9	1.5267	1.75	0.082442	0.16	1.0421	16.3
2	0.0001	0.58844	8.5	0.4908	98.8	1.5000	16.7	0.082306	1.33	0.8721	98.9
1	0.001	0.53822	--	0.00565	--	1.2500	--	0.081215	--	0.0096	--

Table 13. Unsteady accurate solution at Re_C = 2,000, α = 7° with H_f/C = 4%, ε = 0.1%.

Case	Δt (s)	$C_{L,m}$	$E_{j,i-1}$	$C_{L,a} \times 10^{-2}$	$E_{j,i-1}$	St	$E_{j,i-1}$	$C_{D,m}$	$E_{j,i-1}$	$C_{D,a} \times 10^{-3}$	$E_{j,i-1}$
4	0.00001	0.849753	0.74	0.0830	3.37	1.163	0.17	0.114126	0.23	0.02001	3.7
3	0.00005	0.843436	0.95	0.0802	3.9	1.161	0.26	0.113859	0.29	0.01927	4.8
2	0.0001	0.835436	19.03	0.0771	77.04	1.158	10.7	0.113528	7.75	0.01835	79.3
1	0.001	0.676484	--	0.0177	--	1.034	--	0.104730	--	0.00380	--

All errors are in percent.

$\Delta t = 10^{-3}$ s to $\Delta t = 10^{-5}$ s. The relative errors in $C_{L,a}$ and $C_{D,a}$ from $\Delta t = 10^{-3}$ s to $\Delta t = 10^{-5}$ s is reduced from 99.9 to 29.5% and 99.5 to 29.6% at $\alpha = 3°$; 98.8 to 15.3% and 98.9 to 15.2% at $\alpha = 4°$; and 77.04 to 3.37% and 79.3 to 3.7% at $\alpha = 7°$, respectively. However, the downward trend is dependent on the angle of attack. For example, E_{43} of $C_{L,a}$ and $C_{D,a}$, is 3.37 and 3.7% at $\alpha = 7°$; 15.3 and 15.2% at $\alpha = 4°$; 29.9 and 29.6% at $\alpha = 3°$, respectively. This is due to the fact that values of amplitude force coefficients are 1- or 2-order of magnitude lower than the mean values, *i.e.* $C_{L,a} << C_{L,m}$ and $C_{D,a} << C_{D,m}$. Moreover, the reason for which the relative errors of $C_{L,a}$ and $C_{D,a}$ at $\alpha = 3°$ are higher than those of $\alpha = 4°$ and the relative errors of $C_{L,a}$ and $C_{D,a}$ at $\alpha = 4°$ are higher than those of $\alpha = 7°$ is that $C_{L,a \text{ at } \alpha = 3°} << C_{L,a \text{ at } \alpha = 4°} << C_{L,a \text{ at } \alpha = 7°}$ and $C_{D,a \text{ at } \alpha = 3°} << C_{D,a \text{ at } \alpha = 4°} << C_{D,a \text{ at } \alpha = 7°}$.

Based on the data obtained in the Δt independence study shown in Tables 11 to 13, it was decided that a value of 10^{-5} s would be the proper time-step size for the time accurate computations in this Reynolds number. This Δt provides a compromise between accuracy and CPU time. Time steps smaller than $\Delta t = 10^{-5}$ s would noticeably increase the computational time.

Table 14 shows the comparison of CPU time estimated using UAS approach to reach periodic state with $\Delta t = 10^{-4}$ s at $Re_C = 2,000$, with $H_f/C = 4\%$, and $\varepsilon = 0.1\%$ at different angles of attack. The CPU time taken to reach a periodic state is 350, 275, and 50 for 3°, 4°, and 7°, respectively. As can be seen, there is a noticeable difference between the CPU time taken to reach a periodic state, at different angles of attack. The computational time at low angles of attack is much higher than that of the large angles of attack. Note that the unsteadiness and amplitude of the oscillation increases as the angle of attack increases. Thus, at higher angles of attack, the oscillations dominate uniform flow coming from the far-field boundary in a shorter span of time as compared to lower angles of attack. As a result, for small angles of attack at which the level of unsteadiness is low, forming the vortices and establishing periodic oscillations will take more time as compared to higher angles of attack.

OBSERVATIONS

One of the main purposes of the present study is to evaluate the possibility of using QSS approach instead of time accurate computations for the prediction of performance. Many numerical studies used the QSS approach for the prediction of flow over a Gurney flapped airfoil with the assumption that QSS approach has the capability to predict the flow characteristics and the time averaged behavior resulting from time accurate computations with a very good accuracy. Table 15 shows mean lift and drag coefficient errors of QSS approach, *i.e.* with $\Delta t = \infty$, with respect to UAS approach with $\Delta t = 10^{-5}$ s. As shown in Table 15, QSS approach has predicted the mean lift and drag coefficients with errors of 5.5 and 0.67%, 10.6 and 1.67% and 35.9 and 14.83%, at $\alpha = 3°$, 4° and 7°, respectively. As can be seen, the amount of calculated errors is not negligible, and, therefore, QSS approach cannot be used to predict mean lift and drag coefficients with the same accuracy as UAS approach does. In addition, relative errors increase with the angle of attack. For example, the relative error in mean lift and drag coefficients has increased from 5.5 to 35.9% and 0.67 to 14.83%, respectively, by increasing angle of attack from 3° to 7°. This is because the QSS approach introduces the average of flow properties instead of details of flow transient, while UAS approach presents instantaneous flow structure. At higher angles of attack, the flow structure is more complicated, and the vortices which are the main cause of unsteadiness are larger. As a result, the error of QSS approach would be higher with respect to UAS approach due to the fact that QSS approach ignores the capture of these vortices of flow.

Table 15. Relative error of quasi-steady approach with respect to unsteady accurate solution ($Re_C = 2,000$, $H_f/C = 4\%$, $\varepsilon = 0.1\%$).

		E* [%]		
		$\alpha = 3°$	$\alpha = 4°$	$\alpha = 7°$
$\Delta t = \infty$	$C_{L,m}$	5.5	10.6	35.9
	$C_{D,m}$	0.67	1.67	14.83

*This is the error of mean values of force coefficients from QSS approach with respect to UAS approach at $\Delta t = 10^{-5}$ s.

Table 14. Comparison of CPU time taken to reach periodic state using UAS approach with $\Delta t = 10^{-4}$ s for unsteady flow over a Gurney flapped NACA 0008 airfoil at $Re_C = 2,000$, with $H_f/C = 4\%$, and $\varepsilon = 0.1\%$.

α [°]	Average time needed for each linearization iteration (s)	Average number of linearization iterations at each Δt	Overall number of time steps to reach the periodic state	CPU time (h)
3	20	3	21,000	350
4	20	3	16,500	275
7	20	1	9,000	50

In addition, the performance of UIS approach in comparison with that of the UAS approach is also studied. Table 16 shows relative errors of calculated $C_{L,m}$, $C_{D,m}$, $C_{L,a}$, $C_{D,a}$, and St by UIS approach for 3 time steps of 10^{-3}, 10^{-5}, and 5×10^{-5} s with respect to those calculated by UAS approach with $\Delta t = 10^{-5}$ s. Navier-Stokes equations are non-linear by nature, and, in order to have a linear system of equations, convection terms in momentum equations are linearized with respect to mass fluxes ρu and ρv. Therefore, it is necessary to perform the linearization iteration at each Δt in order to reduce the linearization error to the lowest possible amount. As a result, UIS approach in which no linearization iteration is performed does not have the same accuracy as the UAS one.

Table 16 illustrates that, for small time steps, there would be no need to perform linearization iterations. This is reasonable since, when the Δt gets smaller, the error in flow properties between 2 successive time steps becomes lower, and, therefore, the

linearization error decreases. For example, with $\Delta t = 5 \times 10^{-5}$ s, relative errors of calculated $C_{L,m}$, $C_{L,a}$, $C_{D,m}$, $C_{D,a}$, and St by UIS approach with respect to those calculated by UAS approach are 0.29; 2.02; 0.03; 2.23 and 1.02; 0.29, 0.01, 0.04, 0.2, and 0.89; and 0.31; 1.3; 0.25; 1.4 and 0.79, at $\alpha = 3°$, $4°$ and $7°$, respectively. As can be seen, all errors are less than or about 2%.

As observed in Table 16, relative errors decrease as Δt decreases for all parameters studied. For example, relative errors of calculated $C_{L,a}$ by UIS approach with respect to those calculated by UAS approach reduce from 80.7 to 2.02, 15.2 to 0.01, and 5.1 to 1.3 with the decrease in Δt from 1×10^{-3} s to 5×10^{-5} s at $\alpha = 3°$, $4°$ and $7°$, respectively. This shows the limiting trend of all parameters with the decrease in Δt from 1×10^{-3} s to 5×10^{-5} s. Overall, the present results show that UIS approach at small time steps in the order of $\Delta t = 5 \times 10^{-5}$ s or lower is comparable with UAS approach and capable of predicting aerodynamic coefficients with a reasonable accuracy.

Table 17 shows the comparison of CPU time estimated for the solution to reach its periodic nature using UAS and UIS approaches for the case of unsteady flow over a Gurney flapped NACA 0008 airfoil at $Re_C = 2,000$, $\alpha = 7°$, and $H_f/C = 4\%$.

As illustrated in Table 17, the amount of CPU time taken to solve the flow using the UIS approach (100) is approximately 1/3 of that of UAS approach (340). As can be seen, UIS approach at small time steps is capable of producing time-averaged data with less CPU time than UAS approach. Therefore, using UIS approach with small time steps, such as $\Delta t = 5 \times 10^{-5}$ s, can lead to savings in computational cost.

Table 16. Errors of unsteady inaccurate solution with respect to unsteady accurate solution ($R_{eC} = 2,000$, $H_f/C = 4\%$, $\varepsilon = 0.1\%$).

α (°)		E* (%)		
		$\Delta t = 0.001$	$\Delta t = 0.0001$	$\Delta t = 0.00005$
3	$C_{L,m}$	5.3	0.65	0.29
	$C_{L,a}$	80.7	5.1	2.02
	$C_{D,m}$	0.63	0.09	0.03
	$C_{D,a}$	81.01	5.4	2.23
	st	20.4	2.5	1.02
4	$C_{L,m}$	5.3	0.65	0.29
	$C_{L,a}$	15.2	0.54	0.01
	$C_{D,m}$	0.75	0.08	0.04
	$C_{D,a}$	15.4	0.41	0.2
	st	19.1	2.4	0.89
7	$C_{L,m}$	8.6	0.72	0.31
	$C_{L,a}$	5.1	2.5	1.3
	$C_{D,m}$	4.8	0.58	0.25
	$C_{D,a}$	4.4	3.4	1.4
	st	16.8	1.92	0.79

*This is the error with respect to $\Delta t = 10^{5}$ s results from unsteady accurate solution.

EFFECT OF LINEARIZATION CONVERGENCE CRITERION ON THE SOLUTION

The linearization convergence criterion used to stop linearization iteration process was 0.1% in all the simulations presented in the previous sections. In order to ensure that the linearization convergence criterion used to stop linearization iteration process is small enough, simulations of UAS approach are carried out for 3 angles of attack of $\alpha = 3°$, $4°$, and $7°$ with

Table 17. Comparison of CPU time taken to reach periodic state using UAS ($\varepsilon = 0.1\%$, with and $\Delta t = 10^{-5}$ s) and UIS ($\Delta t = 5 \times 10^{-5}$ s) for unsteady flow over a Gurney flapped NACA 0008 airfoil at $Re_C = 2,000$, $\alpha = 7°$ with $H_f/C = 4\%$.

Aproach	Average time needed for each linearization iteration (s)	Average number of linearization iterations in each Δt	Overall number of time steps to reach the periodic state	CPU Time (h)
UIS	20	1	18,000	100
UAS	20	1	61,000	340

linearization convergence criterion values of ε = 0.1, 0.01, and 0.001% at $\Delta t = 10^{-5}$ s. The errors indicated in Fig. 5 are defined as:

$$\Delta_{j,j-1} = \left| C_{L,m_j} - C_{L,m_{j-1}} \right| \qquad (7)$$

$$E_{i,j-1} = \Delta_{i,j-1} / C_{L,m_j} \qquad (8)$$

where: indices 1; 2 and 3 refer to the linearization convergence criterion used for each simulation, *i.e.* ε = 0.1; 0.01 and 0.001%. Note that errors of *St*, $C_{L,a}$, $C_{D,m}$, and $C_{D,a}$ are calculated similarly to the error of $C_{L,m}$, as defined in Eqs. 7 and 8. Figure 5a shows sensitivity of mean lift and drag coefficients calculated from UAS approach to convergence criterion. The relative errors of E_{21} of $C_{L,m}$ and $C_{D,m}$ for 3 angles of attack α = 3°, 4°, and 7° are 0.19; 0.19 and 0.06% as well as 0.03; 0.012 and 0.009%, respectively. The relative errors of E_{32} of $C_{L,m}$ and $C_{D,m}$ are all very small and approximately zero. As can be seen, mean lift and drag coefficients have negligible changes with linearization convergence criterion and, overall, from ε = 0.1% to ε = 0.01%, their changes are less than 0.2%.

Figure 5b shows sensitivity of Strouhal number calculated from UAS approach to convergence criterion. The relative error of E_{21} of *St* for three angles of attack of α = 3°, 4°, 7°, is 0.13; 0.05, and 0.08%, respectively. The relative errors of E_{32} are 0 for all angles of attack. As observed, the *St* also has negligible changes with linearization convergence criterion and, overall, its changes are less than 0.2%, similarly to what has been predicted for mean lift and drag coefficients.

Figure 5c shows sensitivity of amplitude lift and drag coefficients calculated from UAS approach to convergence criterion. The

relative errors of E_{21} of $C_{L,a}$ and $C_{D,a}$ for 3 angles of attack of α = 3°, 4°, 7°, are 6.2; 3.32; 0.85% and 5.84; 3.31; 0.81%, respectively. The relative errors of E_{32} of $C_{L,a}$ and $C_{D,a}$ are all very small and approximately zero. As seen amplitude lift and drag coefficients have different behavior from mean lift and drag coefficients and Strouhal number. The changes in relative errors of $C_{L,a}$ and $C_{D,a}$ from ε = 0.1% to ε = 0.01% (E_{21}) are noticeable and dependent on the angle of attack. As seen in Fig. 5c, the relative errors of E_{21} of $C_{L,a}$ and $C_{D,a}$ decreases when the angle of attack increases. Indeed, amplitude lift and drag coefficients at low angles of attack (α = 3°, 4°) are subjected to major changes, *i.e.* 6.2 and 3.32%; and 5.84 and 3.31%, respectively, than higher angles of attack (α = 7°), which is 0.85 and 0.81%, respectively. This is expected since $C_{L,a\ \text{at}\ \alpha = 3°} << C_{L,a\ \text{at}\ \alpha = 4°} << C_{L,a\ \text{at}\ \alpha = 7°}$ and $C_{D,a\ \text{at}\ \alpha = 3°} << C_{D,a\ \text{at}\ \alpha = 4°} << C_{D,a\ \text{at}\ \alpha = 7°}$.

The tests carried out on the effect of linearization convergence criterion ε show that the relative errors of E21 of $C_{L,m}$, $C_{D,m}$ and *St* undergo minor changes and are all less than 0.2%. However relative errors of E_{21} of $C_{L,a}$ and $C_{D,a}$ have considerable changes, and their changes are dependent on the angle of attack. Overall the relative errors of E_{32} are approximately zero for all parameters at all angles of attack. All in all, it can be concluded that if error of less than 7% is fine enough, then, linearization convergence criterion of ε=0.1% is also an appropriate value to accurately capture unsteady flow field around a Gurney-flapped airfoil at Re_C = 2,000, with H_f/C = 4% and $\Delta t = 10^{-5}$ s. Nevertheless, $\Delta t = 10^{-5}$ s and ε = 0.01% are proper to be used in the computations when transient behavior of the airfoil and amplitude force coefficients are of primary interest.
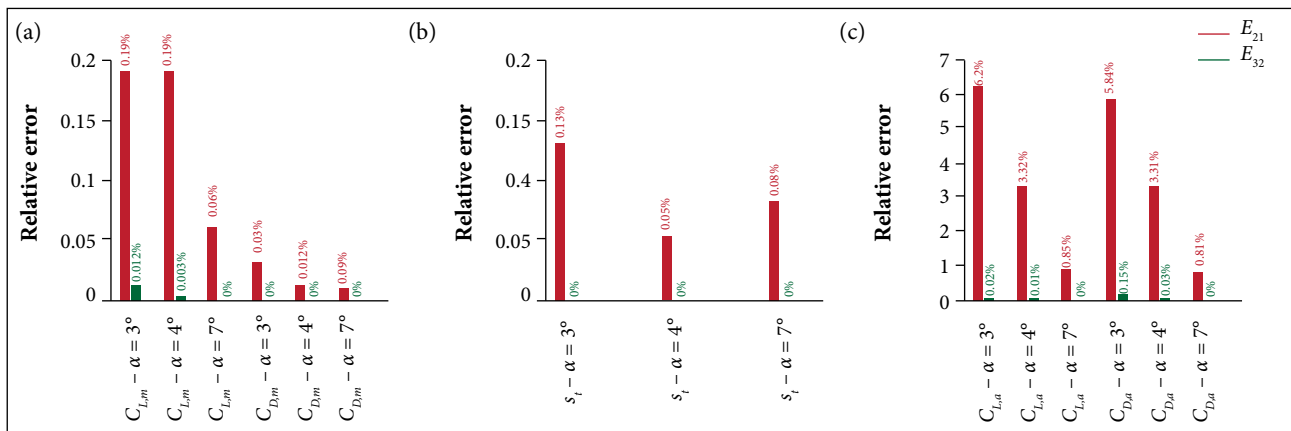
Figure 5. Linearization convergence criterion independence study at $\Delta t = 10^{-5}$ s using UAS for unsteady flow over a Gurney flapped NACA 0008 airfoil at Re_C = 2,000, with H_f = 4%*C*, and α = 3°, 4°, and 7°. (a) Mean values of lift and drag coefficients; (b) Strouhal number; (c) Amplitude of lift and drag coefficients.

CONCLUSION

A detailed study into the aerodynamic behavior of a Gurney flapped NACA 0008 airfoil with a flap height of H_f/C = 4% at angles of attack of 3°, 4°, and 7°, and at ultra-low Reynolds number of Re_C = 2,000 was conducted using a control volume based finite-element collocated scheme. In order to reduce the amount of required memory and to speed up the convergence rate two solver namely band solver and direct sparse solver were examined and their performances were compared with each other. The results showed that the amount of CPU time taken to solve the flow using the sparse solver is 1/27th of that of the band solver. Hence, the sparse solver with node renumbering was used for all computations throughout the present research.

The Δt independence study carried out here demonstrated the importance of proper time-step size selection. All the parameter showed a monotone and asymptotic convergence as Δt decreased. Δt independence study showed that, when the value of 10^{-5} s was employed for the calculations, $C_{L,m}$, $C_{D,m}$ and St were predicted with a very good accuracy and the calculated relative errors were very small. However, the relative errors of $C_{L,a}$ and $C_{D,a}$ were higher in comparison with those of $C_{L,m}$, $C_{D,m}$ and St, depending on the angle of attack. Overall the obtained accuracy with $\Delta t = 10^{-5}$ s is satisfactory providing a compromise between accuracy and CPU time.

Our investigation in this paper showed that for a Gurney flapped airfoil QSS approach is not able to predict the time averaged behavior resulting from UAS approach. The predicted QSS mean parameters showed remarkable discrepancy from those calculated by UAS approach at the regime of ultra-low Reynolds numbers. This is in contrast to what was reported in the literature for Gurney flapped airfoil at higher Reynolds numbers where the flow is turbulent.

Moreover, the present study revealed that results obtained from UIS approach at sufficiently small time steps, were comparable with the results of UAS approach. UIS approach was capable of producing time accurate results with a reasonable accuracy and less CPU time than computationally intensive time accurate simulations.

Finally, simulations of UAS approach at the Δt of 10^{-5} s on the effects of linearization convergence criterion demonstrated that $C_{L,m}$, $C_{D,m}$ and St are not affected by the linearization convergence criterion. However, $C_{L,a}$ and $C_{D,a}$ changed with linearization convergence criterion, and their changes were dependent on the angle of attack. Overall, if error of less than 7% is fine enough, then, linearization convergence criterion of $\varepsilon = 0.1\%$ is a proper value to capture unsteady flow field around a Gurney flapped airfoil. Nevertheless, $\varepsilon = 0.01\%$ is the proper one to be used in the computations especially when transient behavior of the airfoil and amplitude force coefficients are of primary interest.

AUTHOR'S CONTRIBUTION

Khoshlessa M elaborated the idea, performed all the simulations, and prepared all the data and figures. Karimian SMH is the principal investigator of this research, who critically revised the article for important intellectual content and gave the final approval of the version to be published.

REFERENCES

Abdo M (2004) Theoretical and computational analysis of airfoils in steady and unsteady flows (PhD thesis). Montreal: McGill University.

Alisadeghi H, Karimian SMH (2010) Different modelings of cell-face velocities and their effects on the pressure-velocity coupling, accuracy and convergence of solution. Int J Numer Meth Fluid 65(8):969-988. doi: 10.1002/fld2224

Ashby D (1996) Experimental and computational investigation of lift-enhancing tabs on multi-element airfoil. NASA-CR-201482.

Berthelsen PA, Faltinsen OM (2008) A local directional ghost cell approach for incompressible viscous flow problems with irregular boundaries. J Comput Phys 227(9):4354-4397. doi: 10.1016/j.jcp.2007.12.022

Calhoun D (2002) A Cartesian grid method for solving the two-dimensional stream-function vorticity equations in irregular regions.

J Comput Phys 176:231-275. doi: 10.1006/jcph.2001.6970

Coutanceau M, Bouard R (1977) Experimental determination of the main features of the viscous flow in the wake of a circular cylinder in uniform translation. Part 1. Steady flow. J Fluid Mech 79(2):231-256.

Date JC, Turnock SR (2002) Computational evaluation of the periodic performance of a NACA 0012 fitted with a Gurney flap. J Fluid Eng 124:227-234.

Ding H, Shu C, Yeo KS, Xu D (2007) Numerical simulation of flows around two circular cylinders by mesh-free least square-based finite difference methods. International Journal for Numerical Methods in Fluids 53:305-332.

Giguere P, Dumas G, Lemay J (1997) Gurney flap scaling for optimum lift-to-drag ratio. AIAA J 35(12):1888-1890.

Herfjord K (1996) A study of two-dimensional separated flow by a combination of the finite element method and Navier-Stokes equations (PhD thesis). Trondheim: Norwegian Institute of Technology.

Jang CS, Ross JC, Cummings RM (1992) Computational evaluation of an airfoil with a Gurney flap. Proceedings of the 10th AIAA Applied Aerodynamics Conference; Palo Alto, USA.

Jeffrey DRM, Zhang X, Hurst DW (2000) Aerodynamics of Gurney flaps on a single-element high-lift wing. J Aircraft 37(2):295-301. doi: 10.2514/2.2593

Karimian SMH (1994) Pressure-based control-volume finite-element method for flow at all speeds (PhD thesis) Waterloo: University of Waterloo.

Karimian SMH, Schneider GE (1994) Numerical solution of two-dimensional incompressible Navier-Stokes equations: treatment of velocity-pressure coupling. Proceedings of the AIAA 25th Fluid Dynamics Conference; Colorado Springs, USA.

Karimian SMH, Schneider GE (1995) Pressure-based control-volume finite element method for flow at all speeds. AIAA J 33(9):1611-1618. doi: 10.2514/3.12700.

Khoshlessan M (2013) Numerical investigation of unsteady flow over a Gurney flapped airfoil with plunge oscillation (Master's thesis). Tehran: Amirkabir University of Technology.

Khoshlessan M, Karimian SMH, Daemi N (2013) Evaluation of a control-volume based finite-element collocated scheme for the solution of external steady and unsteady incompressible flows at low Reynolds numbers. Proceedings of the 11th International Conference of Numerical Analysis and Applied Mathematics; Rhodes, Greece.

Kunz PJ (2003) Aerodynamics and design for ultra-low Reynolds number flight (PhD thesis). Stanford: Stanford University.

Li Y, Wang J, Zhang P (2002) Effects of Gurney flaps on a NACA 0012 airfoil. Flow Turbulence and Combustion 68(1):27-39.

Liebeck RH (1978) Design of subsonic airfoils for high lift. J Aircraft 15(9):547-561. doi: 10.2514/3.58406

Linnick MN, Fasel HF (2005) A high-order immersed interface method for simulating unsteady compressible flows on irregular domains. J Comput Phys 204(1):157-192. doi: 10.1016/j.jcp.2004.09.017

Liu C, Zheng X, Sung CH (1998) Preconditioned multigrid methods for unsteady incompressible flows. J Comput Phys 139:35-57. doi: 10.2514/6.1997-445

Manish KS, Dhanalakshmi K, Chakrabartty SK (2007) Navier-Stokes analysis of airfoils with Gurney flap. J Aircraft 44(5):1487-1493.

Medjroubi W (2011) Numerical simulation of dynamic stall for heaving airfoils using adaptive mesh techniques (PhD thesis). Oldenburg: Carl von Ossietzky University.

Myose R, Heron I, Papadakis M (1996) The effect of Gurney flaps on a NACA 0011 airfoil. AIAA Paper 1996-0059.

Neuhart DH, Pendergraft Jr OC (1988) A water tunnel study of Gurney flaps. NASA TM-4071.

Ross JC, Storms BL, Carrannanto PG (1995) Lift-enhancing tabs on multi-element airfoils. J Aircraft 32(3):649-655. doi: 10.2514/3.46769

Russel D, Wang ZJ (2003) A Cartesian grid method for modeling multiple moving objects in 2D incompressible viscous flow. J Comput Phys 191:177-205.

Schatz M, Gunther B, Thiele F (2004) Computational modeling of the unsteady wake behind Gurney-flaps. Proceedings of the 2nd AIAA Flow Control Conference, Fluid Dynamics and Co-located Conferences; Portland, USA.

Storms LB, Jang SC (1994) Lift enhancement of an airfoil using a Gurney flap and vortex generators. J Aircraft 31(3):542-547.

Tejnil E (1996) Computational investigation of the low speed S1223 airfoil with and without a Gurney flap (master's thesis). San Jose: San Jose State University.

Tritton DJ (1959) Experiments on the flow past a circular cylinder at low Reynolds numbers. J Fluid Mech 6:547-567.

Troolin DR, Longmire EK, Lai WT (2006) Time resolved PIV analysis of flow over a NACA0015 airfoil with Gurney flap. Exp Fluid 41(2):241-254.

Williamson CHK (1989) Oblique and parallel modes of vortex shedding in the wake of a circular cylinder at low Reynolds numbers. J Fluid Mech 206:579-627.

Xu S, Wang ZJ (2006) An immersed interface method for simulating the interaction of a fluid with moving boundaries. J Comput Phys 216:454-493. doi: 10.1016/j.jcp.2005.12.016